A Novel Design of an Elastance-Controlled Linear Motor-Driven Left Ventricle Simulator

Preston Peak
Texas Heart Institute
Houston, USA
ppeak@texasheart.org

Sai Kode
Texas Heart Institute
Houston, USA
skode@texasheart.org

David Nguyen
Texas Heart Institute
Houston, USA
danguyen@texasheart.org

O.H Frazier
Texas Heart Institute
Houston, USA
OFrazier@texasheart.org

Nobuyuki Kurita
Baylor College of Medicine
Houston, USA
nobuyuki.kurita@bcm.edu

Yaxin Wang
Texas Heart Institute
Houston, USA
ywang@texasheart.org

IECON 2023- 49th Annual Conference of the IEEE Industrial Electronics Society | 979-8-3503-3182-0/23/$31.00 ©2023 IEEE | DOI: 10.1109/IECON51785.2023.10311936

***Abstract*— Mechanical models of the human cardiovascular system exist as test platforms to study the performance of mechanical circulatory systems (MCSs) and interventional cardiac devices *in vitro,* and they must recreate the physiological hemodynamics that would be present inside the human body. This work describes a left ventricle simulator (LVS) that implements a personalized elastance model to control ventricular contraction via a linear motor-driven piston, simulating variable physiological and pathological conditions. The system simulated ventricular and aortic hemodynamics, the Frank-Starling autoregulatory mechanism, atrial kick, and physiological pulsatile flow at varying heart rates for both healthy heart and heart failure conditions. Elastance control not only provides precise motor actuation, but also allows for the simulation of specific heart function, and this work ultimately introduces a novel test platform for heart device validation.**

Keywords—mock circulatory loop, heart model, left ventricle simulator, mechanical circulation

I. Introduction

With 1 in 5 people around the world being affected by heart failure, it is the leading cause of reported death in the world [1, 2]. Interventional devices, artificial heart valves, and especially mechanical circulatory systems (MCSs) are being increasingly used to treat heart disease as the availability of heart donors is limited [3]. MCSs are traditionally part of bridge-to-transplant treatment programs, however they have also found use as permanent solutions in patients [4]. These devices significantly improve patient outcomes, and their development requires sophisticated validation methods to ensure device efficacy prior to *in-vivo* animal and clinical tests [5]. These methods are typically done *in-vitro* using what are essentially complex heart or ventricle simulators, and these simulators are commonly referred to as mock circulatory loops (MCLs).

MCLs traditionally recreate the anatomy and physiology of the human heart by creating pulsatile flow through a mechanical system, and they serve as test platforms for developing MCSs including left ventricular assist devices (LVADs) [5]. They mimic pressure-volume relationships, cardiovascular compliances and resistances, physiological responses of the heart, important pressure waveforms, pulsatile flow, and a wide variety of operational conditions that allow for in depth MCS testing [6, 7]. Though current MCLs focus on MCS testing, early MCLs were developed specifically for artificial heart valve testing, and these systems utilized stepping motors and linear actuators to create an artificial pulse [8, 9]. Later, MCLs became capable of simulating refined compliance and resistance parameters [10], the Frank-Starling autoregulatory mechanism [11], and both systemic and pulmonary circulations [12].

As knowledge of the cardiovascular system profoundly increases, so do the capabilities of modern MCLs [13, 14], and more sophisticated *in-vitro* testing of MCSs and other heart devices has been the result. This work introduces a compact left ventricle simulator (LVS) that takes the sophisticated control and systemic circulation of modern MCLs and utilizes a personalized numerical elastance model to generate pulsatile flow using a linear motor. This model allows for patient specific evaluation of interventional devices and MCSs on a platform that allows for manual adjustment of resistance and compliance parameters and precise actuation during systole and diastole. The novel structural configuration also allows for atrial kick, an important heart function, to be simulated without need for an atrial chamber and a separate linear motor.

The use of elastance control is prevalent in existing literature, as it is a reliable control method [15-17], and this work employs it to additionally allow for simulation of patient-specific heart function given a patient's heart data is accessible. The numerical model used in this work was derived by evaluating the pressure-volume relationship in the left ventricle of a functioning MCL, and it is described by:

$$p(t) = e(t)(V(t) - V_0) \tag{1}$$

In equation 1, $p(t)$ and $V(t)$ represent the pressure and volume in the left ventricle, respectively, over the course of one cardiac cycle, $e(t)$ represents elastance, and V_0 represents the

Research supported by the National Heart, Lung, and Blood Institute of the National Institute of Health under Award Number 1R01HL153538.

volume-axis intercept of the end-diastolic pressure-volume relationship (EDPVR) line. Using this control method, a LVS capable of generating physiological pulsatile flow using a linear motor-driven piston was developed to simulate systemic flow, the Frank-Starling autoregulatory mechanism of the heart, and left ventricular hemodynamics at varying heart rates in a healthy heart (HH) model, a mild heart failure (MHF) model, and a severe heart failure (SHF) model.

II. Materials and Methods

A. Mechanical Construction

The construction of LVS can be separated into the following components: the left ventricle (LV), mitral valve (MV), aortic valve (AoV), aortic compliance (AoC), left ventricular compliance (LVC), systemic vascular resistance (SVR), and systemic vascular compliance (SVC).

The LV was represented by an acrylic block with a hollowed out cylindrical chamber that held a volume of approximately 400 mL. This cylinder guided a piston that pumped fluid without leakage. To prevent backflow in the system, mechanical heart valves (SJM Masters HP Valved Graft, St. Jude Medical, St. Paul, MN, USA) simulated the MV and AoV in their respective locations. Left ventricular contraction was modeled using a linear motor (Electric Thrust, Direct Thrust Designs Ltd, Essex, United Kingdom) to drive a piston that displaced volume within the LV chamber, and the pistons were precisely aligned and fitted with o-rings allow proper actuation and sealing. Additionally, due to the rigidity of the acrylic chamber, a small air chamber was needed to simulate LVC and was machined into the acrylic. Fig. 1 depicts the LV and SVC chamber configuration.

Compliance is an important physiological parameter to recreate when trying to mimic proper hemodynamics. Aside from the small LVC previously mentioned, this work makes use of two compliance chambers that were used to simulate how the volume of arteries and veins changes when pressure changes, as shown in Equation 2.

$$C = \frac{\Delta V}{\Delta P} \tag{2}$$

The AoC was modeled by an air-tight *windkessel* compliance chamber with a trapped air volume of 1140 mL, and the SVC was modeled by a second acrylic block machined into a compliance chamber, shown in Fig. 1. The block was placed on top of the LV, and it acted as an *open-air* compliance chamber with an area of 93.79 cm^2. Open-air compliance is generally greater than windkessel compliance, which is why it was used to model SVC, and the calculation to determine the amount of fluid needed in the open-air chamber is shown in Equation 3.

$$C = \frac{\Delta V}{\Delta P} = \frac{A\Delta h}{\rho g \Delta h} = \frac{A}{\rho g} \tag{3}$$

The windkessel chambers used to simulate LVC and AoC had pockets of trapped air to provide compliance, and the calculation to determine the amount of air trapped in the chambers is described in Equation 4. The ideal gas law was applied, and air temperature and volume remained constant; in addition to atmospheric pressure, pressures in the AoC and LVC chambers were assumed to fluctuate up to 120 mmHg during each contraction.

$$C = \left|\frac{\Delta V}{\Delta P}\right| = \left|\frac{V_1 - V_2}{P_2 - P_1}\right| = \left|\frac{V_2}{P_1}\right| = \left|\frac{V_1}{P_2}\right| \tag{4}$$

Approximate compliance parameters of the LVS system and physiological compliances of the human body are shown in Table 1 [18, 19]. The SVC chamber was uniquely designed and positioned in a way such that it also functioned as the left atrium (LA), and this design was adopted to simulate atrial kick using gravity alone, alleviating the need for an additional linear motor. Furthermore, a Hoffman clamp was secured to the tubing between the AoC and SVC to model SVR, and this clamp was manually adjusted.

The fluid flowed from the LV through the AoV, then into the AoC, then through the SVR, and then into the SVC chamber where it finally flowed through the MV back into the LV. Fluid flow was directed via 1-inch flexible tubing, and a Fig. 1 depicts fluid flow.

TABLE I. Compliance Parameters

	Aortic Compliance	**Systemic Vascular Compliance**	**Ventricular Compliance**
Area (cm^2)	95.03	93.79	0.196
Volume of air (mL)	1140	Open	1.47
Physiological Compliance (mL/mmHg)	~2.5	~118	< 0.1
LVS Compliance (mL/mmHg)	1.3 – 1.5	127.5	< 0.1

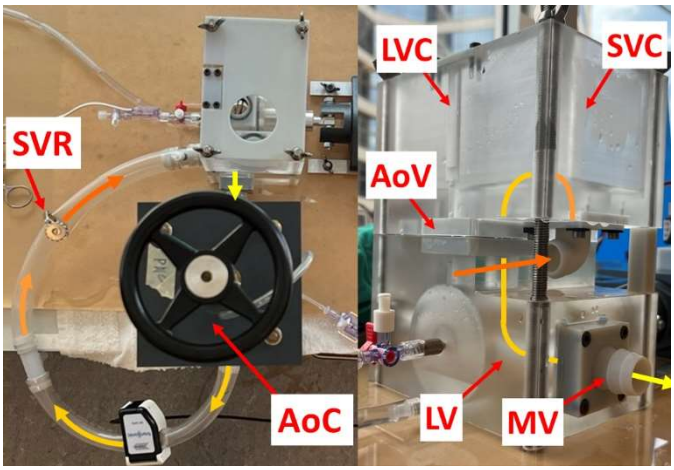

Fig. 1. Labeled photos of the left ventricle simulator, and depiction of flow through the system. SVR, systemic vascular resistance; AoC, aortic compliance; LVC, left ventricular compliance; AoV, aortic valve; LV, left ventricle; MV, mitral valve; SVC, systemic vascular compliance.

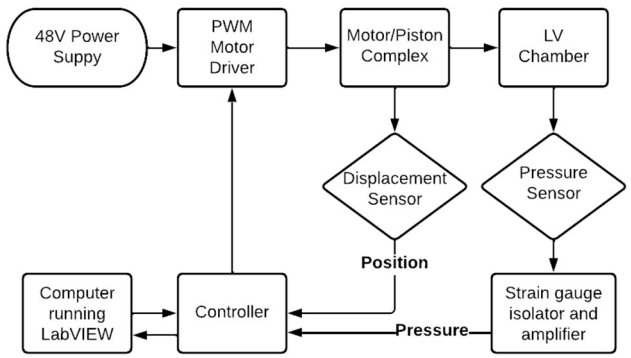

Fig. 2. Schematic of the communications between the electrical components of the LVS.

B. Electrical Components

Linear motor actuation was controlled by a PWM motor driver (Junus JSP-090-10, Copley Controls, Canton, MA, USA) programmed to convert an analog input into a PWM signal with a varying duty cycle. The duty cycle was calculated as a ratio between the input voltage (-10V to 10V range) and 10V (e.g. 5V input results in a 50% duty cycle). This motor driver received input signals from a data acquisition device (DAQ) (NI USB-6002, National Instruments, Austin, TX, USA) and was powered by a 48V power supply (PMT-48V350W1AR, Delta Electronics Inc., Fremont, CA, USA).

A diagram of communication between the electrical components is shown in Fig. 2. In addition to controlling the PWM motor driver, the DAQ received signals from sensors in the LVS. Pressure transducers (TruWave, Edwards Lifesciences, Irvine, CA, USA) measured pressures in the LV and aorta, and a displacement transducer (LT-M-0100-S-L, Gefran, Provaglio d'lseo BS, Italy) attached to the top of the linear motor measured the displacement of the piston. This displacement measurement was used to calculate the fluid volume in the LV. Additionally, a flow probe (ME 16PXL, Transonic Systems, Ithaca, NY, USA) was placed after the AoC to calculate the generated flow in the system.

C. Software & Controller Design

The Frank-Starling autoregulatory mechanism of the heart is an important property to simulate heart function that describes the relationship between pressure and volume in the heart. The controller used in the LVS was centered around manipulating pressure-volume relationship in the LV chamber to match that of a human heart, and LabVIEW was used to implement this control algorithm. A closed-loop system determined DAQ output to the PWM motor driver by implementing a numerical elastance function that determined target LV pressures during a simulated cardiac cycle.

Fig. 3 shows the elastance function used to simulate the HH condition graphically over the course of 1 second (60 BPM heartrate). The elastance function was divided into two equations that represented systole and diastole separately, and adjusting heart rate in the system not only manipulated the function duration, but also the systolic percentage (SP). The SPs used at each heart rate are present in Table 2 in the results section, and they were calculated using Equation 5 [20].

$$SP = \frac{541-2.2HR}{1000} \times \frac{HR}{60} \quad (5)$$

Using this model to control LV hemodynamics required the instantaneous *volume* and *time* since the cardiac cycle began, and its output was a theoretical PV-loop that was tracked via the controller.

Two PID controllers were implemented via LabVIEW and controller design is shown in Fig. 4; the theoretical pressure calculated by the elastance function operated as the setpoint, and the experimental pressure measured in the LV was the process variable. One PID controller was used during systolic contraction, while another was used during diastolic relaxation. The reason being is that there was a great difference in forces needed between diastole and systole, so different PID controllers allowed for precise control. PID tuning was done in the time domain via Ziegler and Nichols' tuning method, and based on the error between theoretical and experimental pressures, the PID output variable was voltage sent from the DAQ to the PWM motor driver. Effective actuation resulted from these methods.

The LVS simulated a HH condition, MHF condition, and SHF condition in this study. Each of these states was tested at 60, 75, 95, 120 and 140 BPM to simulate different physiological scenarios, i.e. sleep, walking and exercise, and to simulate MHF and SHF, the elastance function was scaled down in the y-direction by 70% and 50%, respectively. Data was collected on the LV pressure-volume loops (PV-loops), LV pressure waveforms, aortic pressure waveforms, Frank-Starling response of the system, and flow rates.

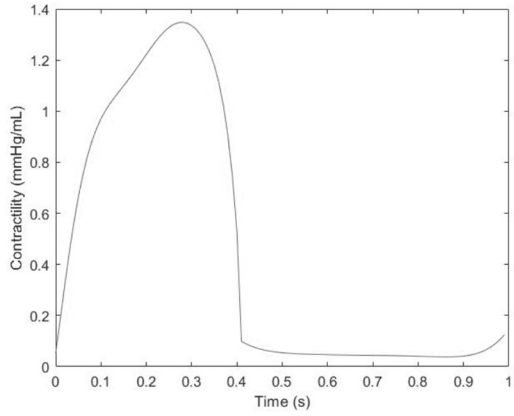

Fig. 3. Numerical elastance function used to control LVS function. X-axis is time (s) and Y-axis is contractility (mmHg/mL)

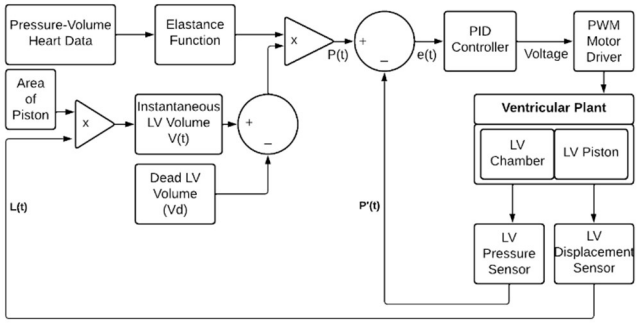

Fig. 4. Schematic of the controller design.

III. Results

A. HH Left Ventricular Pressure-Volume Loops

Fig. 5, depicts the experimental healthy heart PV-loop traces of the LVS at 60, 75, 90, 120, and 140 BPM. The theoretical loops present on the graphs were established by the elastance controller.

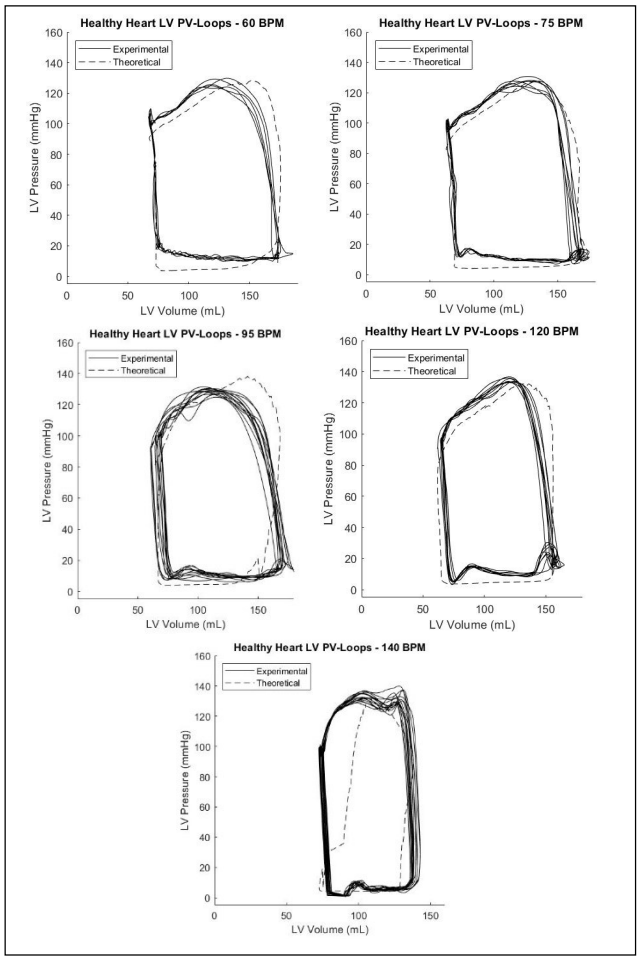

Fig. 5. LVS pressure-volume loops at a healthy heart condition for the tested heart rates of 60, 75, 95, 120, and 140 BPM.

TABLE II. System Hemodynamics for a Healthy Heart Condition

	LVS Hemodynamics (Healthy Heart)				
	60 BPM	*75 BPM*	*95 BPM*	*120 BPM*	*140 BPM*
Systolic Percent (%)	41	47	53	55	54
Mean Arterial Pressure (mmHg)	93	88	91	96	91
Resistance (dynes·sec·cm^{-5})	1760	1302	1128	1025	860
Flow (L/min)	4.0	5.1	6.1	7.1	8.0

B. HH Ventricular & Aortic Hemodynamics

The LV and aortic pressure waveforms for each tested heart rate at the HH condition are depicted in Fig. 6, and Table 2 presents the compiled parameters and results of each test run.

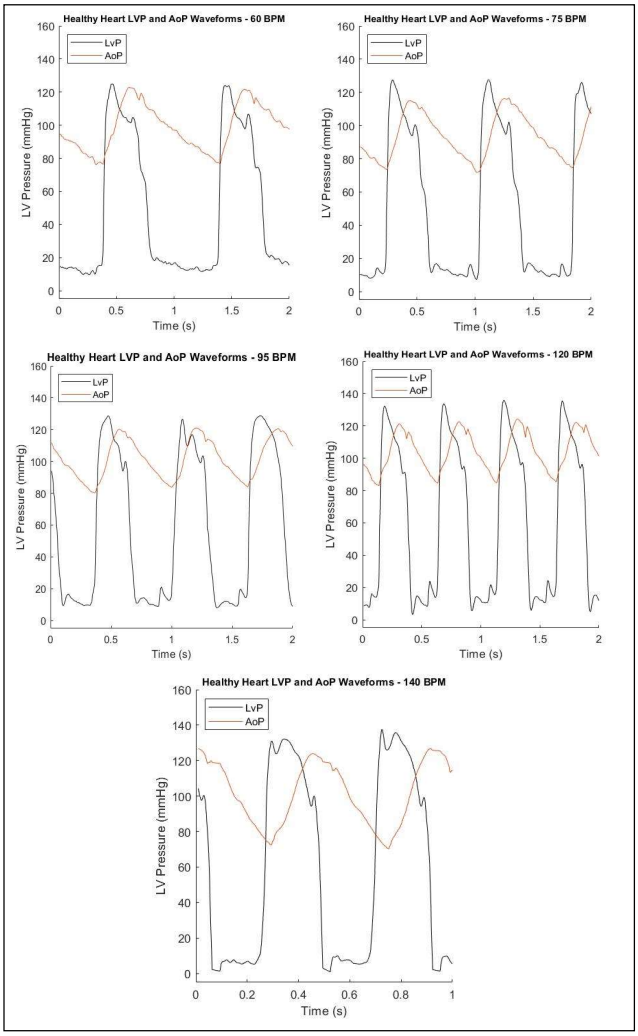

Fig. 6. Left ventricle and aortic pressure waveforms at a healthy heart condition for the tested heart rates of 60, 75, 95, 120, and 140 BPM.

C. The Frank-Starling Mechanism

The Frank-Starling curves for the HH condition at each tested heart rate were gathered, and Fig. 7 depicts the gathered curves and shows how the ESPVR lines were calculated. Additionally, Table 3 lists the HH ESPVR slopes at each heart rate. The mean HH ESPVR was 1.21 ± 0.03.

TABLE III. End Systolic Pressure-Volume Relationships

	LVS ESPVRs (Healthy Heart)				
HR (BPM)	60	75	95	120	140
ESPVR slope	1.25	1.20	1.16	1.20	1.22

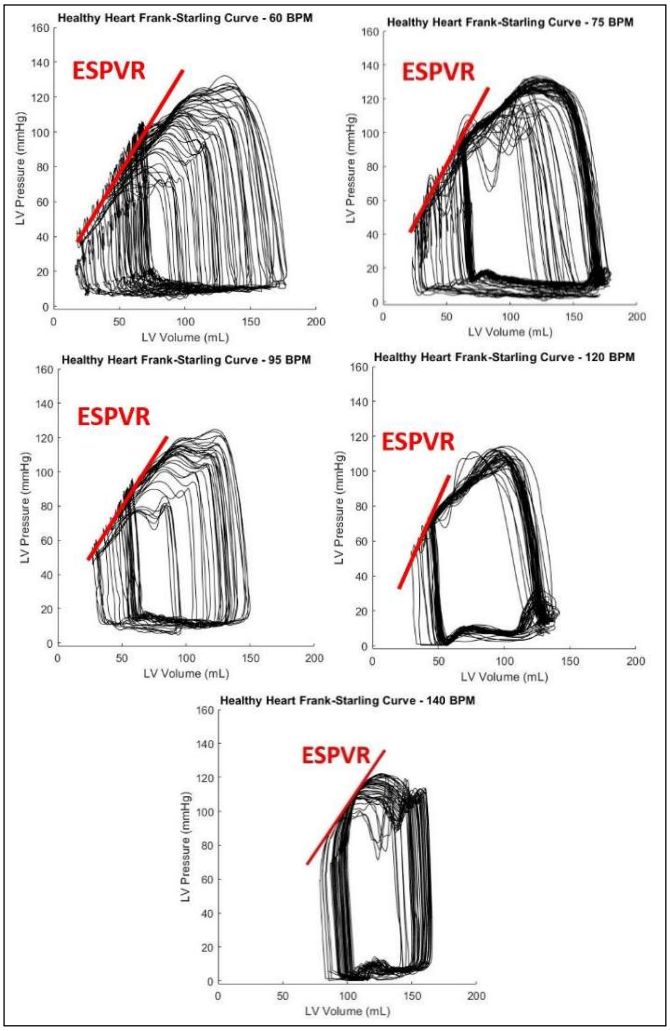

Fig. 7. Frank-Starling curves at a healthy heart condition for the tested heart rates of 60, 75, 95, 120, and 140 BPM.

D. Mild and Severe HF Hemodynamics & Frank-Starling

The LVS performance when simulating MHF and SHF conditions at 75 BPM are depicted in Fig. 8, and Table 4 compares these results to those of a HH at 75 BPM. This table includes the calculated ESPVR slopes for each condition.

TABLE IV. SYSTEM HEMODYNAMICS FOR THE HEART FAILURE CONDITIONS AT 75 BPM

	LVS Hemodynamics (75 BPM)		
	Healthy Heart	*Mild Heart Failure*	*Severe Heart Failure*
Mean Arterial Pressure (mmHg)	88	75	63
Resistance (dynes·sec·cm^{-5})	1302	1333	1856
Flow (L/min)	5.1	4.2	2.5
ESPVR slope	1.2	1.0	0.8

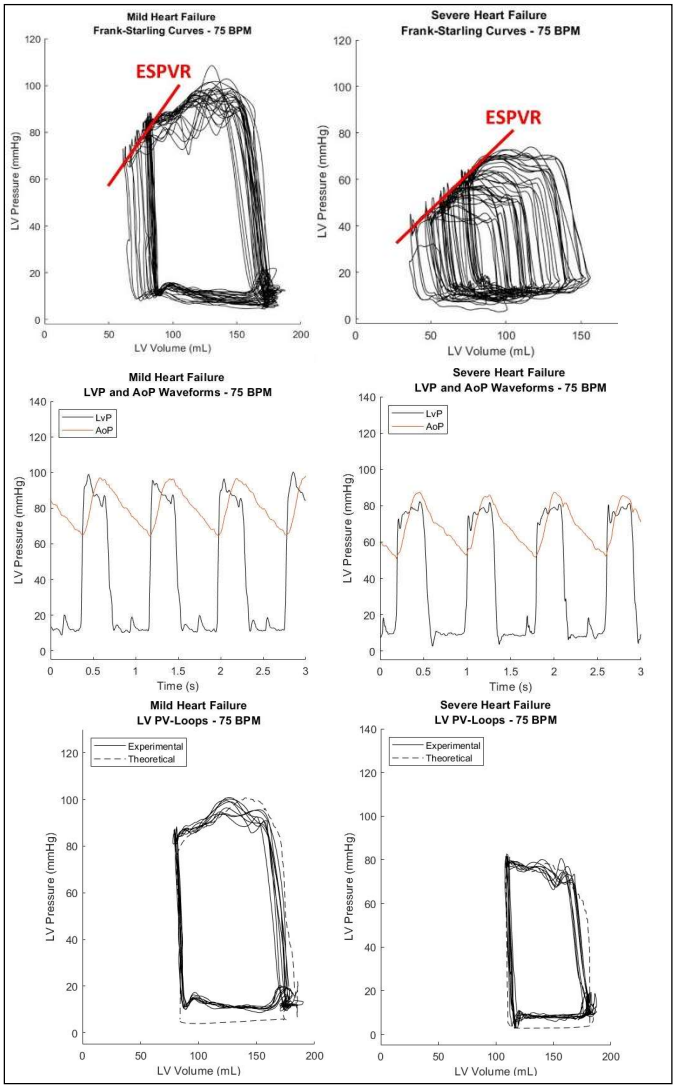

Fig. 8. Hemodynamic results in the LVS at both a mild and severe heart failure condition. Mild heart failure results are in the left column, and severe heart failure results are in the right column.

IV. DISCUSSION

A. System Hemodynamics

Using an elastance-based control algorithm to determine linear motor movement successfully allowed for the LVS system to recreate ventricular and aortic hemodynamics. Cardiac output and flow rate increased at each heart rate tested, and the LVS had the capacity to pump greater than 10 L/min. This means the loop was properly designed and assembled for high flow situations. Additionally, during mild and severe HF simulations, flow rates dropped as expected.

PV-loops established in the LV traced the theoretical loops well for the HH, MHF, and SHF models aside from occasional pressure dips and spikes during systole, and physiological volume displacements and high-end target pressures were reached. These dips and spikes can be attributed both to friction preventing quick piston movement and to the reactiveness of the systolic PID coefficients which cause pressures to overshoot after isovolumetric contraction. Additionally, at lower heart

rates (as seen in Fig. 7) during diastolic contraction, the end diastolic pressures never fully reached the low-end target pressures, and this was a result of a high venous return volume in the SVC which exerted pressure into the chamber as it fills. This did not appear to be an issue at higher heart rates (see Fig. 9), and this was due to there being increased motor actuation force during relaxation. This ultimately allowed low-end target pressures to be reached.

Just as target pressures were reached in the LV, the aortic pressures were also within physiological targets. The systolic and diastolic aortic pressure difference at each test condition should be approximately 40 mmHg, and at the HH condition, aortic pressure differences ranged from 37 to 53 mmHg. This difference of 53 mmHg was at 140 BPM, and larger pressure differences are suitable for higher heart rates. For the MHF and SHF conditions, the aortic pressure differences were 32 and 36 mmHg, respectively, with an overall decrease in pressures compared to the HH model. A shortcoming of the system's pressure waveforms was the slight lag between LV and aortic pressure peaks. The aortic pressure sensor was approximately 10 cm downstream of the aortic valve, and measuring pressure closer to the valve may improve this.

The Frank-Starling autoregulatory mechanism was tested by observing heart function as preload was adjusted, and this response functioned very well. The left ventricular ESPVR line varies from person to person, but what is certain is that as heart function deteriorates, the ESPVR slope decreases [21, 22]. For the HH condition, cardiac output increased as preload was increased, and the calculated ESPVR slopes were very similar. Not only did the heart failure conditions give similar results, but HH ESPVR lines had slopes steeper than those of the MHF ESPVRs; similarly, MHF ESPVR lines had steeper slopes than the SHF condition. Note, however, that physiological ESPVR lines should become concave to the volume axis as cardiac output increases to its upper limits [23], and these upper limits were not able to be tested at this developmental stage. Therefore, the lines appear linear, and the SVC must be made to hold more fluid than is currently possible.

The configuration of the two chambers, with the SVC being on top of the LV was a stark improvement to previous iterations that lack simulation of atrial kick. Without this mechanism, diastolic filling of the ventricle was hindered, and pressures veered into the negative, as shown in Fig. 9 [16].

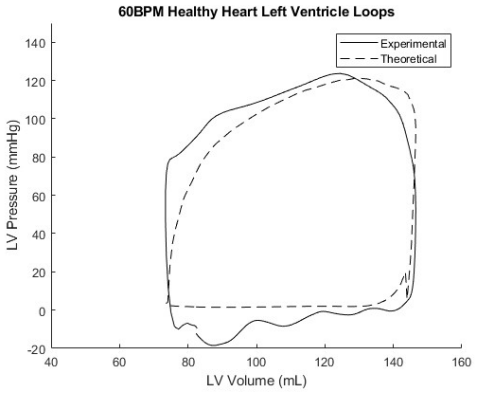

Fig. 9. Pressure-volume loop of the LV at 60 BPM when there is no atrial kick.

B. *Future Directions*

Limitations mentioned in the previous section may be addressed with simple controller and structural tuning, and introducing PID self-tuning methods may be a more efficient manner of improving control. Additionally, PID gains scheduling should be an effective way of reducing pressure spikes and dips during the cardiac cycle.

Currently, the next steps are to test the device at both higher and lower heart rates as well as introduce specific physical and internal conditions. The physical conditions may include rest, exercise, standing up, sitting down, and falling, and internal conditions include various stages of heart left/right heart failure, septal defects, valve regurgitation, and Fontan heart configuration.

The elastance-control method was highly effective for basic control and Frank-Starling simulation, and in the future, the numerical model will be replaced with derived elastance models of different animal and human hearts. The current heart failure models were achieved by simply scaling down the HH elastance function, so to gather heart data from a patient with left, right, or total heart failure will allow further development of a LVS that can recreate personalized heart functions and provide a capable test environment for heart devices.

V. Conclusions

This work described a novel LVS system that can simulate personalized heart function via elastance control. The resulting hemodynamics and ESPVRs of the system at a wide range of heart rates for HH, MHF, and SHF conditions show the stability and robustness of the LVS, and the results both outlined areas to be improved and showed that the LVS shows great promise as a testing platform.

Acknowledgment

Research was supported by the National Heart, Lung, and Blood Institute of the National Institute of Health under Award Number 1R01HL153538.

References

1. Lloyd-Jones, D.M., et al., *Lifetime risk for developing congestive heart failure: the Framingham Heart Study.* Circulation, 2002. **106**(24): p. 3068-72.
2. Virani, S.S., et al., *Heart Disease and Stroke Statistics-2020 Update: A Report From the American Heart Association.* Circulation, 2020. **141**(9): p. e139-e596.
3. Vitali, E., et al., *Mechanical circulatory support in severe heart failure: single-center experience.* Transplant Proc, 2004. **36**(3): p. 620-2.
4. Christiansen, S., A. Klocke, and R. Autschbach, *Past, present, and future of long-term mechanical cardiac support in adults.* J Card Surg, 2008. **23**(6): p. 664-76.
5. Cappon, F., et al., *Mock circulatory loops used for testing cardiac assist devices: A review of*

computational and experimental models. Int J Artif Organs, 2021. **44**(11): p. 793-806.
6. Gregory, S.D., et al., *An advanced mock circulation loop for in vitro cardiovascular device evaluation.* Artif Organs, 2020. **44**(6): p. E238-E250.
7. Timms, D.L., et al., *A compact mock circulation loop for the in vitro testing of cardiovascular devices.* Artif Organs, 2011. **35**(4): p. 384-91.
8. Cornhill, J.F., *An aortic--left ventricular pulse duplicator used in testing prosthetic aortic heart valves.* J Thorac Cardiovasc Surg, 1977. **73**(4): p. 550-8.
9. Wieting, D.W., et al., *Design of a system for analyzing flow behavior of prosthetic human heart valves.* Cardiovasc Res Cent Bull, 1966. **5**(2): p. 41-56.
10. Reul, H., et al., *Hydromechanical simulation of systemic circulation.* Med Biol Eng, 1974. **12**(4): p. 431-6.
11. Koenig, S.C., et al., *Hemodynamic and pressure-volume responses to continuous and pulsatile ventricular assist in an adult mock circulation.* ASAIO J, 2004. **50**(1): p. 15-24.
12. Kolff, W.J., *Mock circulation to test pumps designed for permanent replacement of damaged hearts.* Cleve Clin Q, 1959. **26**: p. 223-6.
13. Gehron, J., et al., *Development and Validation of a Life-Sized Mock Circulatory Loop of the Human Circulation for Fluid-Mechanical Studies.* ASAIO J, 2019. **65**(8): p. 788-797.
14. Nestler, F., et al., *A hybrid mock circulation loop for a total artificial heart.* Artif Organs, 2014. **38**(9): p. 775-82.
15. Baloa, L.A., J.R. Boston, and J.F. Antaki, *Elastance-based control of a mock circulatory system.* Ann Biomed Eng, 2001. **29**(3): p. 244-51.
16. Peak, P., et al., *Physiological Control Algorithm for a Pulsatile-flow 3D Printed Circulatory Model to Simulate Human Cardiovascular System.* Annu Int Conf IEEE Eng Med Biol Soc, 2022. **2022**: p. 4005-4009.
17. Yaxin, W., et al., *Replication of pressure-volume loop with controllable ESPVR and EDPVR curves on a personalized mock circulatory loop based on elastance function.* Annu Int Conf IEEE Eng Med Biol Soc, 2017. **2017**: p. 1282-1286.
18. Tanaka, T., et al., *Compliance of human pulmonary "venous" system estimated from pulmonary artery wedge pressure tracings--comparison with pulmonary arterial compliance.* Jpn Circ J, 1986. **50**(2): p. 127-39.
19. Thenappan, T., et al., *The Critical Role of Pulmonary Arterial Compliance in Pulmonary Hypertension.* Ann Am Thorac Soc, 2016. **13**(2): p. 276-84.
20. Boudoulas, H., et al., *Linear relationship between electrical systole, mechanical systole, and heart rate.* Chest, 1981. **80**(5): p. 613-7.
21. Grossman, W., et al., *Contractile state of the left ventricle in man as evaluated from end-systolic pressure-volume relations.* Circulation, 1977. **56**(5): p. 845-52.
22. Mehmel, H.C., et al., *The linearity of the end-systolic pressure-volume relationship in man and its sensitivity for assessment of left ventricular function.* Circulation, 1981. **63**(6): p. 1216-22.
23. Gregory, S.D., et al., *Replication of the Frank-Starling response in a mock circulation loop.* Annu Int Conf IEEE Eng Med Biol Soc, 2011. **2011**: p. 6825-8.